Heliyon 8 (2022) e11045

Contents lists available at ScienceDirect

Heliyon

journal homepage: www.cell.com/heliyon

Research article

Development of solar isodose lines: Mercatorian and spatial guides for mapping solar installation areas

Stephen Ndubuisi Nnamchi [a,*], Mustafa Muhamad Mundu [b]

[a] Department of Mechanical Engineering, SEAS, Kampala International University, P.O. Box 20000, Kampala, Uganda
[b] Department of Electrical, Telecommunication and Computer, SEAS, Kampala International University, P.O. Box 20000, Kampala, Uganda

HIGHLIGHTS

- The Solar Power Potential (SPP) concentrated areas are enclosed by maximum isodose line.
- The SPP concentrated areas are useful for the installation of efficient solar facilities.
- The effective mercatorian coordinates bounding SPP concentrated areas were determined from the SPP contours.
- The concentrated districts were identified with the aid of effective mercatorian coordinates.
- The effective mercatorian and spatial isodose lines enhance the accuracy of solar facilities installation.

ARTICLE INFO

Keywords:
Isodose
Mercatorian coordinate
Spatial coordinate
Distributed and concentrated SPP
Distributed and concentrated areas
Solar facilities

ABSTRACT

Mercatorian and spatial studies of solar power potential (SPP) provide technical guides for mapping actual solar installation areas for the efficient performance of photovoltaic plants. Acquisition and processing of satellite and on-station data on clearness index, relative sunshine hours, latitude, longitude and SPP preceded their modeling and simulations. The mercatorian SPP model is a geometric function of latitude and longitude, whereas the spatial SPP model is a function of x and y coordinates developed from the Haversine formula. Multiple isodose lines and a single maximum isodose line characterized the distributed and concentrated SPP contours, respectively. The present geometric SPP model validated well with the measured SPP with insignificant error results for the study areas. The Concentrated SPPs: 757.5, 635.2, 557.5 and 405.9 W/m^2 with their corresponding percentage concentrated areas (actual): 28.85(29084.6), 41.48(15368.6), 4.37(1179.6) and 0.75(635.7)%(m^2) for Northern Region (NR), Eastern Region (ER), Central Region (CR) and Western Region (WR), respectively. These results support the efficient performance of solar facilities within the confine of the SPP concentrated areas. The effective mercatorian coordinates were useful in identifying districts within the SPP concentrated areas. Furthermore, the high magnitude of the SPP in ER and NR supports that they are favored for the installation of solar facilities.

1. Introduction

The industrial and domestic energy demand socio-economic growth of the society is attracting exploitation of natural energy resources like the solar energy using the helio-photovoltaic plant in the conversion of solar to electrical energy. The magnitude of solar power potential or global solar radiation defines the potential of a place to hold an helio-photovoltaic plant. In case of limited measurement of solar power potential (SPP), a mathematical model quantifies the value of SPP for a region.

Generally, the direct linear relationship between the normalized SPP and the clearness index dominates the solar power potential (SPP) model. Essentially, the clearness index signifies the intensity or magnitude of the cloud within the study area [1, 2, 3, 4, 5, 6, 7]. The input parameters of the SPP model include temperature, altitude and sunshine hours, longitude, clearness index, wind speed and extraterrestrial radiation [8, 9, 10, 11, 12, 13, 14, 15, 16, 17].

Commonly, relative sunshine hours (RSH) is a linear function of the clearness index [18, 19, 20], the quadratic function of relative sunshine hours [21, 22, 23, 24, 25], and polynomials of relative sunshine hours

* Corresponding author.
E-mail addresses: stephen.nnamchi@kiu.ac.ug (S.N. Nnamchi), mundu.mustafa@kiu.ac.ug (M.M. Mundu).

https://doi.org/10.1016/j.heliyon.2022.e11045
Received 1 August 2022; Received in revised form 22 September 2022; Accepted 7 October 2022

2405-8440/© 2022 The Author(s). Published by Elsevier Ltd. This is an open access article under the CC BY-NC-ND license (http://creativecommons.org/licenses/by-nc-nd/4.0/).

and temperature, relative humidity, precipitation and latitude [17, 26, 27, 28, 29, 30, 31, 32, 33, 34, 35, 36]. The linear, quadratic and polynomial SPP models in literature [18, 19, 20, 21, 22, 23, 24, 25, 26, 27, 28, 29, 30, 31, 32, 33, 34, 35, 36] are none geometric and uncoordinated; hence, it is associated with ample truncation errors, which affect the accuracy of the SPP model. Therefore, there is a need to develop a robust SPP model in geometric and coordinate forms, which minimizes the truncation error in the bid to improve the accuracy of the coordinated SPP models (mercatorian and spatial SPP models). The uncoordinated SPP models cannot develop a contour or an isopleth that brings about isodose lines necessary for defining solar facility installation areas.

Besides, the model development of the SPP, the empirical studies of the SPP are achieved by stationing measurement equipment like pyranometer, pyrheliometer, sunshine recorders and geographic information systems, GIS [37, 38, 39], but the coverage is highly limited because of the high cost of extensive installation of recording equipment. However, the present work develops a geometric and quadratic SPP model using relative sunshine hours, latitude and longitude. The relative sunshine hours designate the extraterrestrial condition of the study areas, while the latitude and longitude designate the terrestrial characteristics of the study areas. The clearness index model encompasses both terrestrial and extraterrestrial conditions of the study areas against the bulk of clearness models in the literature [18, 19, 20, 21, 22, 23, 24, 25, 26, 27, 28, 29, 30, 31, 32, 33, 34, 35, 36, 37, 38, 39], which are solely modeled on the extraterritorial characteristic of the study areas.

Moreover, the present model distinctively formulates the relative sunshine hours as a geometric function of latitude and longitude, in the bid to make the SPP model mercatorian or sensitive to both latitude and longitude of the study areas. Also, the present work transforms the mercatorian SPP model into the spatial model using the Haversine formula to generate an SPP model dependent on the spatial coordinates (x, y) [40, 41].

The installation of solar facilities is highly technical. Thus, installing a solar facility based on the avalanche of discrete SPP or global solar radiation data could result in the underperformance of the solar facility. The underperformance may be due to the offset installation of the solar plants outside the areas with high solar irradiance. Lines of constant or equal solar irradiance, known as isodose lines, enclose the study areas. The actual areas with a highly concentrated isodose are determined from the contours of the SPP. This gives the actual areas available for the installation of the solar facility. Once the installation of the solar facilities employs the concentrated isodose and its areas, the solar facility (plant) is likely to perform. Unfortunately, this information cannot be availed by the avalanche of satellite and station-measured SPP data. Developing the distributed and concentrated isodose lines from the bulk of the satellite or measured data provides this important technical information.

Consequently, this paper presents the art of developing distributed and concentrated SPPs from satellite data. The mercatorian and spatial isodose contours are useful for identifying districts with high SPP and determining the size of the distributed and concentrated areas, respectively. Strategically, the concentrated areas are ideal for the installation of solar facilities. Hence, using effective mercatorian and spatial coordinates established by maximum isodose line, this paper maps out SPP concentrated areas for proper installation and efficient performance of solar facilities, and equally identifies the districts within the SPP concentrated areas.

2. Material and methods

2.1. Study areas

The study areas cover the entire territory of Uganda, composed of four regions, the Northern Region (NR), the Eastern Region (ER), the Central Region (CR) and the Western Region (WR) covering 241551, 85392, 39479, 61403 and 55277 km^2, respectively. The regions: NR, ER, CR and WR are at an elevation of 1073, 1143, 1200 and 1473 m, respectively, above mean sea level (MSL) [42]. The difference in elevation is partly responsible for the variations in the geographic characteristics of these regions. Uganda is an equatorial sub-Saharan country, landlocked in the north by Southern Sudan, in the east by Kenya, in the west by Congo and in the south by Rwanda and Tanzania. By being an equatorial country, Uganda is suitable for installing solar facilities. According to Fig. 1, the NR region is composed of five sub-regions: West Nile, Acholi, Karamoja and Lango. The ER comprises Teso, Elgon and East-Central subregions. The CR is made up only of the Central subregion. The Western and South Western form the WR.

2.2. Methodology

The material and methods commenced with the acquisition of the essential and primary input data for the development of the SPP and normalized solar power potential (NSPP) models. The acquired data are clearness index (k_T), relative sunshine hours (RSH), latitude (ϕ), longitude (λ), solar power potential (SPP) from the National Aeronautic Space Administration (NASA) and Department of Physics, Makerere University, which furnished the satellite and on-station data, respectively. Filtration and arrangement of satellite data in the Excel environment and export to OriginLab yielded the coefficients of the SPP, NSPP, RSH, and k_T models. Figs. 2 and 3 show the algorithm for the methodology. Sequentially, the SPP model is developed as a function of k_T, the k_T model is developed as a function of the RSH, ϕ and λ. In the same vein, the RSH model is established as a function of ϕ and λ. Subsequently, the k_T model nests the RSH model, while the mercatorian SPP model (MSPP) model nests the k_T model. Furthermore, the mercatorian coordinates are converted into the Cartesian (spatial) coordinates (x, y) to obtain the equivalent spatial SPP model (SSPP) using the Haversine formula. Formulating mercatorian and spatial models, MSPP and SSPP respectively fulfill the set objective of the present study. The output parameters of the analysis in the flow chart are: *SPP*, *areas* (A_d and A_c), ϕ, λ, x and y. These essential results aid in the detailed investigation of the solar power distribution (Fig. 2) and concentration (Fig. 3) within the study areas.

2.2.1. Description of flowcharts

The distributed and concentrated SPP flowcharts in Fig. 2 and Fig. 3, respectively accomplish the development of the isodose lines.

2.2.2. The distributed SPP flowchart

The flowchart in Fig. 2 is initiated by inputting the latitude (ϕ_i), longitude (λ_i), relative sunshine hours (RSH_i), measured/satellite: clearness index ($K_{T,i}$) and solar power potential (SPP_i) for the four regions {NR, ER, CR, WR}. The maximum and minimum of ϕ_i and λ_i are sorted ($\phi_{\min}$, $\lambda_{\min}$, $\phi_{\max}$, $\lambda_{\max}$). These extreme coordinates establish the distributed boundary conditions. Then, clearness index (K_T) and modified clearness index (K_T) models are developed using the input data. The dimensionless SPP is directly proportional to the clearness index modified (K_T). The Haversine formula converts the mercatorian coordinates into spatial coordinates. Essentially, the magnitude of mercatorian SPP corresponds to that of spatial SPP, but the coordinates differ. In addition, the emergence of spatial coordinates helps in the computation of the magnitude of the distributed and concentrated areas. Lastly, the measured SPP validate the simulated SPP. On completion of computations or iterations for the four regions within the study areas, the algorithm displays the important output results and stops.

2.2.3. The concentrated SPP flowchart

The concentrated SPP flowchart (Fig. 3) is a subset of the distributed SPP flowchart (Fig. 2) representing areas with maximum SPP. The concentrated SPP flowchart is a simple algorithm solely responsible for identifying districts within concentrated SPP. The algorithm starts by

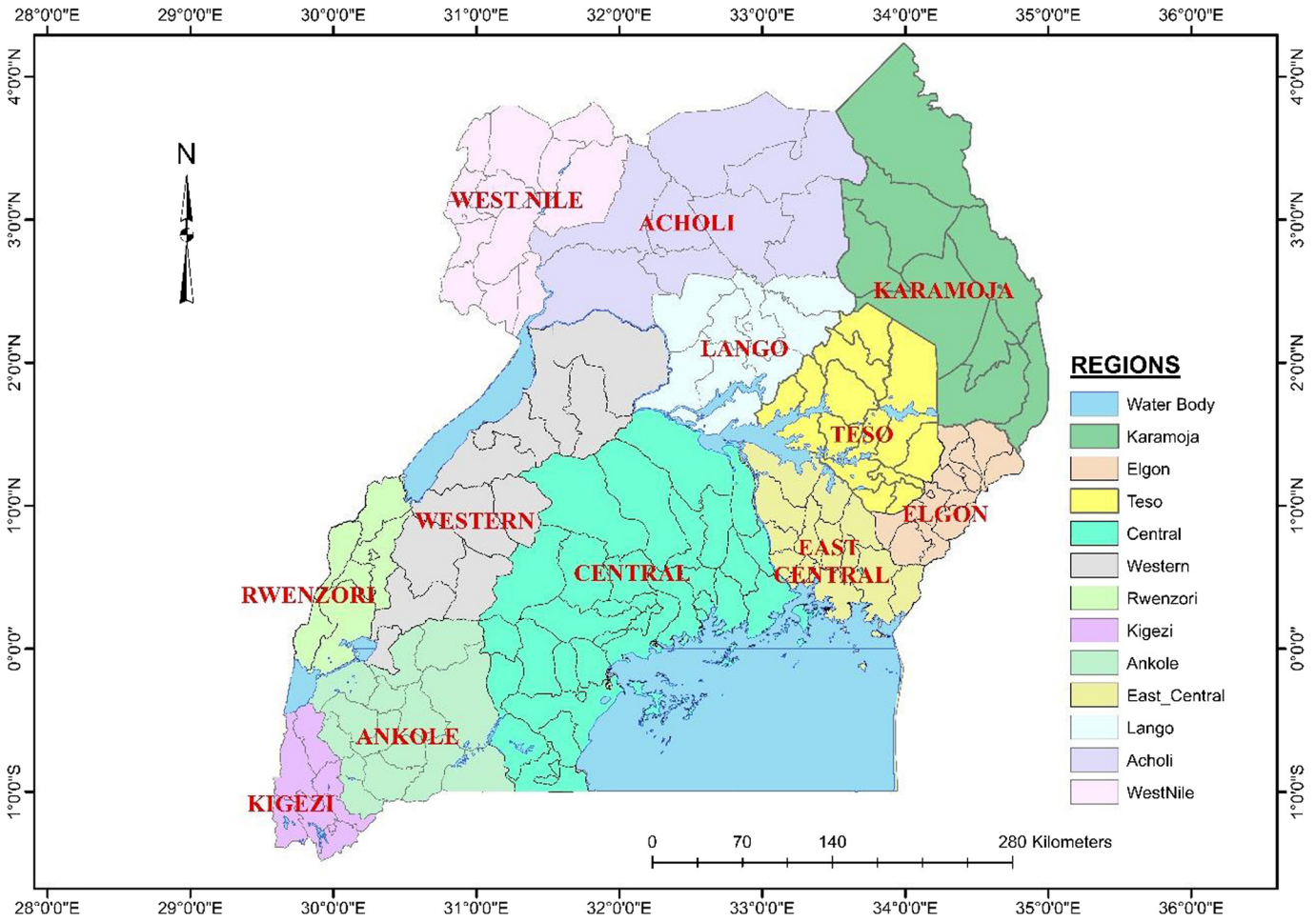

NR ≡ {West Nile, Acholi, Karamoja, Lango}; ER ≡ {Teso, Elgon, East Central}; CR ≡ {Central}; WR ≡{Western, South Western}

Fig. 1. Map of the study areas (NR, ER, CR, WR).

accepting initial input data as in the distributed SPP flowchart. The algorithm uses four boundary equalities (forming the boundaries of the maximum concentrated SPP or isodose line enclosure) in identifying favorable districts. At the same time, it rejects the districts outside the maximum concentrated SPP. On completion of the iterations in Fig. 3, it outputs the districts with maximum concentrated SPP and their mercatorian coordinates.

2.3. Formulation of solar power potential (SPP) model

The direct mathematical relationship between the solar power potential and clearness index in Eq. (1) formulates the SPP model. The solar power potential (SPP) is synonymous with global solar radiation (H) reaching the horizontal or inclined surface. It is a ratio of the terrestrial to extraterrestrial solar power reaching a horizontal surface, which is equivalent to the clearness index of a location [36, 43] in Eq. (1)

$$\frac{SPP}{SPP_0} = \frac{\overline{SPP}}{\overline{SPP_0}} \equiv \frac{H}{H_0} = \frac{\overline{H}}{\overline{H_0}} = k_T \tag{1}$$

where, H is the monthly daily solar irradiance reaching a horizontal surface, H_0 is the corresponding monthly average daily extraterrestrial solar irradiance on the same location, whereas $\overline{H}$ is the average monthly average daily solar irradiance reaching a horizontal surface and $\overline{H_0}$ is the corresponding average monthly average daily extraterrestrial solar irradiance in the same location, k_T, is the clearness index of a given location.

The clearness index, k_T is modeled as a function of latitude and relative sunshine hours (RSH) in accordance with [44] as represented in Eq. (2). Mubiru et al. [10], Rijix and Huskley [11] developed the previous clearness index models for the study areas. Mubiru et al. [10] recommend the quadratic model as the best of their models for the study areas in Eq. (2)

$$k_T = a_0 + a_1 RSH + a_2 RSH^2(-) \tag{2}$$

where a_l, $l = 0, 1, 2$ are coefficients of Eq. (2) and RSH is the relative sunshine hours.

Rijix and Huskley [11] recommend a linear model for the study areas in Eq. (3)

$$k_T = b_0 + b_1 RSH(-) \tag{3}$$

where b_l, $l = 0, 1$ are coefficients of Eq. (3)

However, the present work has proposed a more robust clearness index model, which incorporates the latitude, longitude and relative sunshine hours of the study areas in Eq. (4) as

$$k_T = c_0 + c_1 \cos\phi + c_2 \sin\lambda + c_3 RSH + c_4 \cos\phi.\sin\lambda + c_5 RSH\cos\phi + c_6 RSH.\sin\lambda + c_7 \cos^2\phi + c_8 \sin^2\lambda + c_9 RSH^2 + \epsilon_{K_T}(-) \tag{4}$$

where, c_l, $l = 0, 1, 2, \ldots, 9$ are the coefficients of the cubic k_T model, ϕ is the latitude, λ is the longitude within the study areas and ϵ_{K_T} is the truncation error associated with the clearness model in Eq. (4).

The quadratic function of latitude and longitude defines the RSH in Eq. (5)

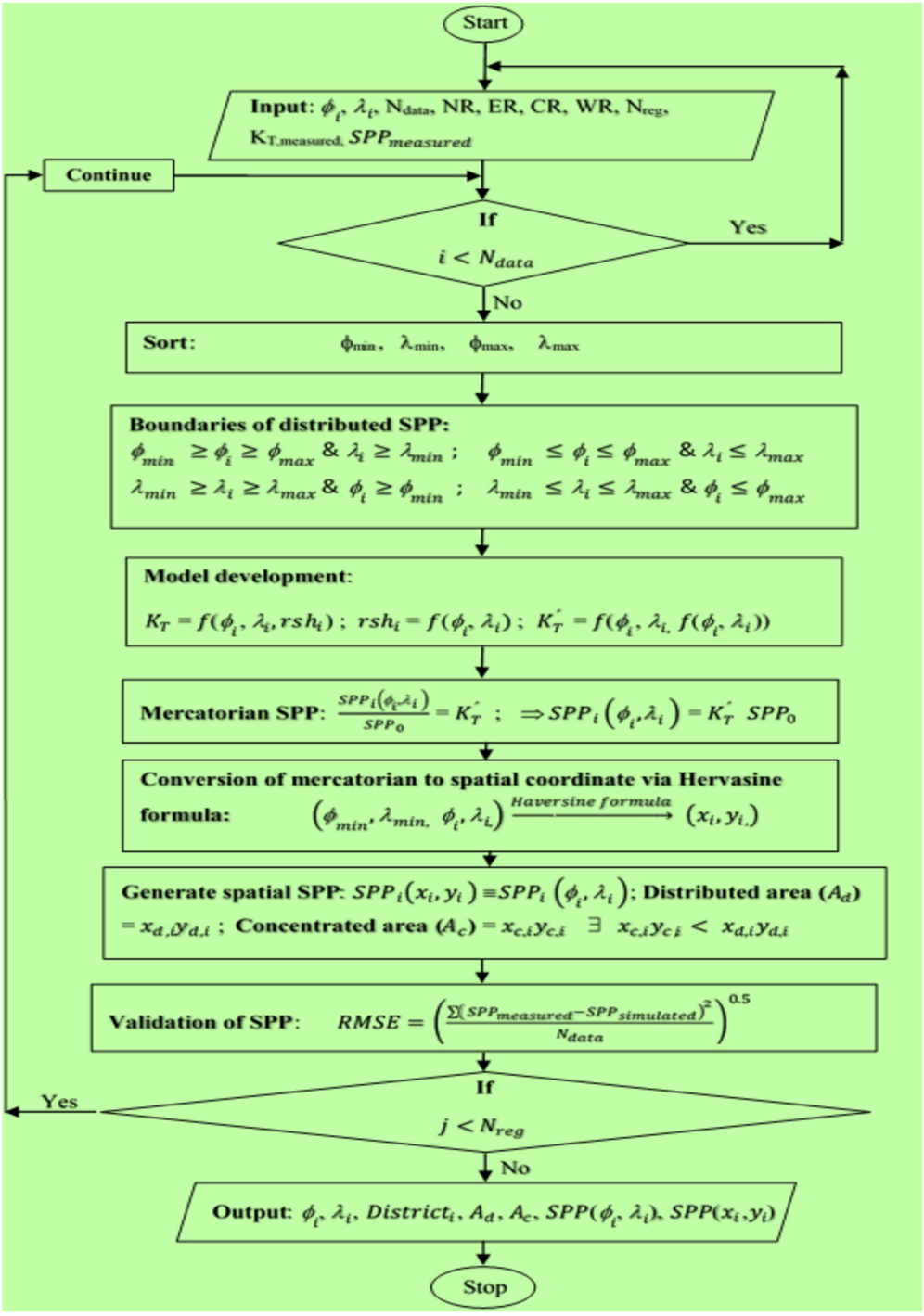

Fig. 2. Distributed SPP flowchart.

$$RSH = d_0 + d_1\cos\phi + d_2\sin\lambda + d_3\cos\phi.\sin\lambda + d_4\cos^2\phi + d_5\sin^2\lambda + \epsilon_{RSH} \quad (5)$$

where, d_l, $l = 0, 1, \ldots, 5$ are coefficients of the quadratic RSH model, λ is the longitude of a given location and ϵ_{RSH} is the truncation error accompanying the RSH model in Eq. (5).

Substituting Eq. (5) into Eq. (4) gives Eq. (6) which depends on the latitude and longitude of the location

$$k_T = c_0 + c_1\cos\phi + c_2\sin\lambda + c_3\left(d_0 + d_1\cos\phi + d_2\sin\lambda + d_3\cos\phi.\sin\lambda + d_4\cos^2\phi + d_5\sin^2\lambda\right) + c_4\cos\phi.\sin\lambda + c_5\left(d_0 + d_1\cos\phi + d_2\sin\lambda + d_3\cos\phi.\sin\lambda + d_4\cos^2\phi + d_5\sin^2\lambda\right).\cos\phi + c_6\left(d_0 + d_1\cos\phi + d_2\sin\lambda + d_3\cos\phi.\sin\lambda + d_4\cos^2\phi + d_5\sin^2\lambda\right).\sin\lambda + c_7\cos^2\phi + c_8\sin^2\lambda + c_9\left(d_0 + d_1\cos\phi + d_2\sin\lambda + d_3\cos\phi.\sin\lambda + d_4\cos^2\phi + d_5\sin^2\lambda\right)^2 + \epsilon_{K_T}(-) \quad (6)$$

Equation (6) modifies Eq. (1) in Eq. (7a), which is a mercatorian representation of the SPP model depending on the latitude and longitude of a location.

$$\frac{SPP}{SPP_0} = \frac{\overline{SPP}}{\overline{SPP_0}} \equiv \frac{H}{H_0} = \frac{\overline{H}}{\overline{H_0}}$$

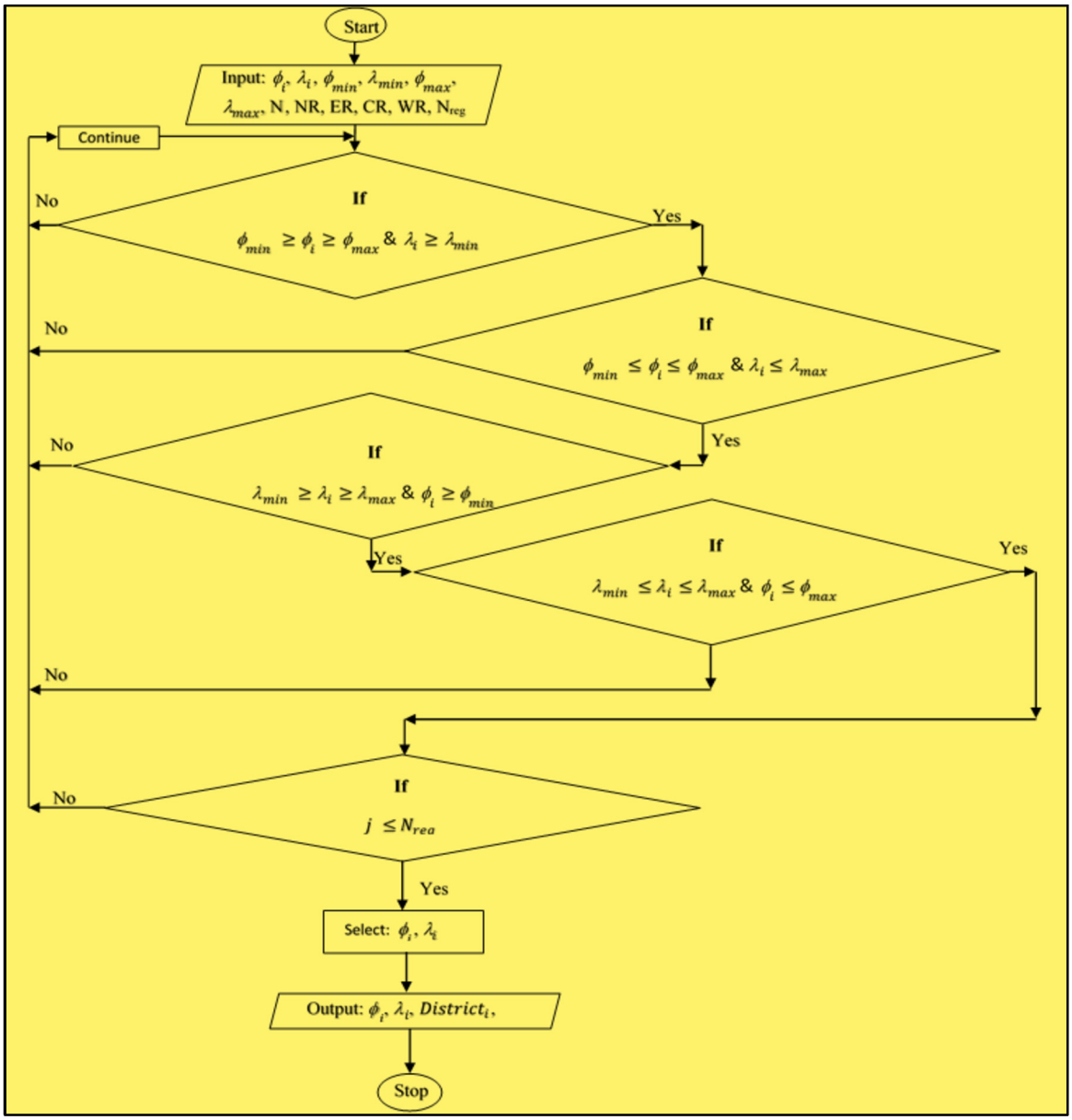

Fig. 3. Concentrated SPP flowchart.

$$
\begin{aligned}
&= c_0 + c_1\cos\phi + c_2\sin\lambda + c_3\left(d_0 + d_1\cos\phi + d_2\sin\lambda\right.\\
&\quad + d_3\cos\phi.\sin\lambda + d_4\cos^2\phi + d_5\sin^2\lambda\left.\right) + c_4\cos\phi.\sin\lambda\\
&\quad + c_5\left(d_0 + d_1\cos\phi + d_2\sin\lambda + d_3\cos\phi.\sin\lambda + d_4\cos^2\phi\right.\\
&\quad + d_5\sin^2\lambda\left.\right).\cos\phi + c_6\left(d_0 + d_1\cos\phi + d_2\sin\lambda + d_3\cos\phi.\sin\lambda\right.\\
&\quad + d_4\cos^2\phi + d_5\sin^2\lambda\left.\right).\sin\lambda + c_7\cos^2\phi + c_8\sin^2\lambda\\
&\quad + c_9\left(d_0 + d_1\cos\phi + d_2\sin\lambda + d_3\cos\phi.\sin\lambda + d_4\cos^2\phi\right.\\
&\quad + d_5\sin^2\lambda\left.\right)^2 + \epsilon_{K_T}(-)
\end{aligned}
\tag{7a}
$$

Similarly, Muburi et al. [10] proposed the SPP model in Eq. (7b) as

$$
\begin{aligned}
\frac{SPP}{SPP_0} = \frac{\overline{SPP}}{\overline{SPP_0}} \equiv \frac{H}{H_0} = \frac{\overline{H}}{\overline{H_0}} &= a_0 + a_1 RSH + a_2 RSH^2\\
&= 0.288 + 0.154RSH + 0.448RSH^2(-)
\end{aligned}
\tag{7b}
$$

Equation (7c) provides equivalent SPP models by Rijix and Huskley [11] as

$$
\frac{SPP}{SPP_0} = \frac{\overline{SPP}}{\overline{SPP_0}} \equiv \frac{H}{H_0} = \frac{\overline{H}}{\overline{H_0}} = b_0 + b_1 RSH = 0.24 + 0.47RSH(-) \tag{7c}
$$

Equation (8) gives the average daily, monthly extraterrestrial solar irradiance [45] as follows;

$$
H_0 = I_{sc}\left[1 + 0.033\cos\left(\frac{360n}{365}\right)\right]\left[\cos\phi\cos\delta\sin\omega_s + \frac{2\pi\omega_s}{360}\sin\phi\sin\delta\right]
$$
$$
\exists SPP_0 \equiv H_0 \tag{8}
$$

where I_{sc} is the solar constant (1367 W m^{-2}), n is the number of days starting from the first January, ω_s is the sunset hour angle, ϕ is the latitude of a given location and δ is the angle of declination defined in Eq. (9) according to [45] as

$$
\delta = 23.45\sin\left[360\left(\frac{284 + n}{365}\right)\right] \tag{9}
$$

and ω_s is the sunset hour angle expressed in Eq. (10)

$$
\omega_s = \cos^{-1}(-\tan\delta\tan\phi) \tag{10}
$$

Table 1. Descriptive statistics of input variables used in the analysis [54, 55].

Variable	Region							
	NR		ER		CR		WR	
	Mean	Std. dev.	Mean	Std. dev.	Mean	Std. dev.	Mean	Std. dev.
$SPP_{satellite}$ (W/m^2)	731.14	25.36	637.05	51.03	496.90	23.83	360.79	12.12
$SPP_{measured}$ (W/m^2)	727.83	25.23	530.39	41.70	494.71	23.72	358.99	12.06
K_T (–)	0.57	0.02	0.58	0.02	0.62	0.03	0.51	0.02
RSH (–)	0.58	0.04	0.59	0.03	0.48	0.05	0.46	0.03
ϕ (°)	2.70	0.53	1.07	0.45	0.52	0.36	0.70	0.62
λ (°)	32.73	1.14	33.86	0.44	31.94	0.77	30.52	0.59

Haversine formula in Eq. (6) determines the geographical distance, $d_{i,j}$ between any two locations [46, 47, 48, 49, 50] by converting the mercatorian model into the spatial form using Eq. (11)

$$d_{ij} = 2R_{Earth}.Atan2\left[\left(\sin^2\left(\frac{\phi_2-\phi_1}{2}\right)+\cos\phi_1\cos\phi_2\sin^2\left(\frac{\lambda_2-\lambda_1}{2}\right)\right)^{0.5},\left(1-\left(\sin^2\left(\frac{\phi_2-\phi_1}{2}\right)+\cos\phi_1\cos\phi_2\sin^2\left(\frac{\lambda_2-\lambda_1}{2}\right)\right)\right)^{0.5}\right]$$
$$\exists x_{i,1} = x_{i-1,1} + d_{i,1};\ y_{1,j} = y_{1,j-1} + d_{1,j} \quad (11)$$

where R_{Earth} is the radius of the Earth (a perfect sphere) equal to 6371 km [46, 51, 52, 53], d_{ij} (km) is the distance separating the two locations; (ϕ_1, λ_1) and (ϕ_2, λ_2) are the latitudes and longitudes of the locations, respectively, x (km) is the distance in the x-direction and y (km) is the distance in the y-direction.

The measured SPP validates the simulated SPP in Equation (7) using root mean square error, RMSE in Eq. (12)

$$RMSE = \left(\frac{(SPP_{measured} - SPP_{simulated})^2}{N}\right)^{0.5} \quad (12)$$

where SPP is the solar power potential (W/m^2) and $N(-)$ is the number of data observed.

Equation (13) defines the percentage of concentration of the SPP (PC_SPP) as follows:

$$\text{PC\_}SPP = \frac{SPP\ concentrated\ area}{SPP\ distributed\ area} \times 100 = \frac{d_{i1,con}d_{1j,con}}{d_{i1,dis}d_{1j,dis}} \times 100(\%) \quad (13)$$

3. Results and discussions

The tables (Tables 1–6) and figures (Figs. 4(a, b)-7(a, b) and Figs. 8–15) sequentially present the results duly discussed in this section.

3.1. Statistical analysis of input data

The statistical analysis of input variable data centers on the mean and the standard deviation. The mean in Table 1 projects the central value of the input variables, whereas the standard deviation in Table 1 describes the dispersion or deviation of various data from the mean value. The high value of standard deviation implies that there is much error or discrepancy associated with the data set and vice versa.

3.2. Results of model coefficients

The normalized solar power potential (*NSPP*) models in Eqs. (6) and (7) are represented by a second-order geometric equation with the coefficients (c_l, $l = 1, \ldots, 9$ in Table 2) for the regions (Northern, Eastern, Central and Western). The nested coefficients (d_l, $l = 1, \ldots, 5$ in Table 3) designate the *RSH* in Eqs. (4) and (5). The coefficients of the models are limited to the study areas since the data used to determine them are sensitive to the geographic characteristics of the study areas. Therefore, the coefficients are not valid for study areas with different geographic characteristics. Moreover, the SPP model assumes that truncation error is infinitesimal, for that reason, the analysis excludes it. The coefficient of determination for the models is approximately one. It indicates a strong association between *NSPP* and mercatorian indicators (latitude and longitude). Further, the results substantiate the fact that mercatorian variables are properly selected and reflect the SPP and NSPP [15, 24]. The *NSPP* or *SPP* model is equivalent to the clearness index in Eqs. (1) and (7) which is a nonlinear geometric function of the relative sunshine hours, latitude and longitude of the study areas as shown in Tables 1 and 2 with a strong coefficient of determination buttressing the fact that the latitude and longitude explicitly represent the relative sunshine hours. Substituting the relative sunshine hours in Eq. (5) into Eq. (4) makes Eq. (6) depend on the latitude and longitude. Thus, on specifying latitude and longitude in Eq. (6), develops *NSPP* or *SPP* on a regional basis. The areas with a high *NSPP* or *SPP* are depicted in the mercatorian plot [15, 24].

Table 2. Coefficients of normalized solar power potential in Eq. (7).

Coefficient	Regions			
	NR	*ER*	*CR*	*WR*
c_0	4.84E-10	−3.37E-09	−5.07E-08	1.07E-08
c_1	2.71E-01	2.71E-01	3.25E-01	2.71E-01
c_2	3.23E-11	−2.99E-11	−4.00E-10	1.22E-10
c_3	5.20E-01	5.20E-01	6.24E-01	5.20E-01
c_4	−3.28E-11	2.93E-11	4.00E-10	−1.23E-10
c_5	2.52E-11	−4.77E-11	−2.33E-10	1.70E-10
c_6	−9.28E-13	−4.05E-14	1.64E-12	−2.05E-12
c_7	4.89E-10	−3.36E-09	−5.08E-08	1.07E-08
c_8	9.15E-13	5.40E-13	−1.15E-12	1.85E-12
c_9	2.25E-13	−1.61E-13	−4.05E-13	9.21E-13
R^2	1.00	1.00	1.00	1.00

Table 3. Coefficients of relative sunshine hours in Eq. (5).

Coefficient	Regions			
	NR	*ER*	*CR*	*WR*
d_0	−35618.944	44.1060	159668.095	131.060
d_1	72085.362	−87.627	−322779.589	−261.689
d_2	−1395.893	−0.004	6908.606	−0.033
d_3	1455.681	1.000	−6996.559	1.000
d_4	−36483.021	43.522	163134.361	130.637
d_5	−51.959	0.003	86.171	0.032
R^2	0.800	1.000	0.800	1.000

3.3. Identification of SPP concentrated areas (districts)

Figs. 4(a, b)-7(a, b) present both the distributed and concentrated SPP for *NR*, *ER*, *CR* and *WR*, respectively. According to Figs. 4(a, b) and

Table 4. Distribution and concentration of solar power potential in Figs. 4(a, b)-7(a, b).

Region	Distributed areas (km^2)	Concentrated areas (km^2)	Percentage of concentration (%)	Remarks
NR	100800	29084.65	28.85	Based on Figs. 4(a, b)
ER	37050	15368.64	41.48	Based on Figs. 5(a, b)
CR	26790	1179.59	4.37	Based on Figs. 6(a, b)
WR	84760	635.70	0.75	Based on Figs. 7(a, b)

Table 5. Districts concentrated with solar power potential in Figs. 4(a, b)-7(a, b).

Region	ϕ_{min}	ϕ_{max}	λ_{min}	λ_{max}	Districts captured by the concentrated isodose line	Conc. SPP (W/m^2)	Remarks
NR	1.6	3.0	19.3	35.0	Abim (2.73,33.7), Agago (), Alebtong (2.83,33.3), Amolatar (1.63,32.8), Amudat (1.95,34.9), Amuru (2.82,31.9), Apac (1.98,32.5), Dokolo (1.92,33.2), Gulu (2.77,32.3), Kaabong (2.73,33.7), Kole (2.40,32.8), Lira (2.33,33.1), Moroto (2.53,34.7), Nakapiripirit (1.92,34.6), Napak (2.20,34.3), Nebbi (2.45,31.3), Nwoya (2.63,32.0), Omoro (2.72,32.5), Otuke (2.50,33.5), Oyam (2.23,32.4), Pader (2.83,33.1), Pakwach (2.46,31.5), Zombo (2.50,30.9)	743.7-757.5	Based on Figs. 4(a, b) and 8
ER	0.3	2.0	34.5	34.7	Bududa (1.02,34.4), Bukwo (1.27,34.7), Kapchorwa (1.33,34.6), Kween (1.41,34.5), Manafwa (1.02,34.3), Mbale (0.95,34.3), Ngora (1.49,33.8), Serere (1.50,33.5), Soroti (1.72,33.5), Kaberamaido (1.70,33.2), Katakwi (1.97,34.1)	624.7-635.2	Based on Figs. 5(a, b) and 9
CR	0.9	1.3	32.7	33.3	Kyankwanzi (1.20,31.8), Nakaseke (1.22,32.1), Kiboga (0.97,31.7), Kayunga (0.99,32.9), Nakasongola (1.35,32.4)	543.8-557.5	Based on Figs. 6(a, b) and 10
WR	−0.8	1.32	31.9	32.0	Kisoro (1.22,29.6)	403.5-405.9	Based on Figs. 7(a, b) and 11

8, *NR* is concentrated with high SPP ($743.7 \leq SPP \leq 757.5\ W\,m^{-2}$). Considering the selected districts within the *NR* (Abim Agago, Alebtong, Amolatar, Amudat, Amuru, Apac, Dokolo, Gulu, Kaabong, Kole, Lira, Moroto, Nakapiripirit, Napak, Nebbi, Nwoya, Omoro, Otuke, Oyam, Pader, Pakwach and Zombo in Table 5), indicates that nonlinear SPP model (Eq. (7)) is effective for determining quality SPP data for the development of isodose in the region [14]. Broadly, Figs. 5(a, b) and 9 show that the SPP model for the Eastern Region, which is capable of identifying the following concentrated districts; Bududa, Bukwo, Kapchorwa, Kween, Manafwa, Mbale, Ngora, Serere, Soroti, Kaberamaido and Katakwi in Table 5. The installation of solar facilities should target districts endowed with high SPP ($624.7 \leq SPP \leq 635.2\ W\,m^{-2}$). However, the present solar power plant in the Tororo district is outside the favored districts within the Northern Region in Table 5. Thus, Tororo the plant cannot generate much power relative to the identified districts in the Northern region. Essentially, solar power developers and planners should concentrate on the identified districts to boost solar power generation in the nation (Uganda).

Correspondingly, Figs. 6(a, b) and 10 identified the following districts; Kyankwanzi, Nakaseke, Kiboga, Kayunga and Nakasongola with moderate SPP ($543.8 \leq SPP \leq 557.5\ W\,m^{-2}$) and should be included in the solar exploitation list. Consistently, Figs. 7(a, b) and 11 identified Kisoro district with low SPP ($403.5 \leq SPP \leq 405.9\ W\,m^{-2}$) should be excluded from the solar exploitation list of Uganda.

Moreover, Table 4 and Eq. (13) provide the concentrated (and distributed) SPP areas, which are useful for the installation of solar facilities as follows: 29084.648 (100800), 15368.638(37050), 1179.585(26790) and 635.7(84760) km^2 for NR, ER, CR and WR, respectively. Offset installations will eventually culminate in the underperformance of the solar plants. These results show that high SPP and more expanse of land for installing solar facilities characterize ER and NR compared to CR and WR. The installation of the solar facility should be discouraged in the WR as the magnitude of SPP and the concentrated areas are least compared to other regions.

3.4. Validation of SPP model results

Figs. 12–15 present the fitting of the present and past SPP models in the study areas (NR, ER, CR and WR). The present model is in good agreement with the measured data than the previous models. The Root Mean Square Error (RMSE) validates this investigation in Table 6. The RMSE of the present work compared to those of Rijix and Huskley [11] and Mubiru et al. [10] is quite insignificant which implies that the present model is more robust for prediction of the SPP, development of concentrated and distributed SPP isodose lines for the study areas. The robustness of the SPP model further portrays that the variables used in the modeling and simulation are well selected and suited for the geographic characteristics of the study areas. These variables (latitude, longitude, clearness index and relative sunshine hour) are effective for the definition of the SPP in the present study areas and other study areas having similar latitude and elevation from the mean sea level.

3.5. Application of results

Based on the SPP result obtained in this study, the present work has shown that the installation of solar power plants in the Western Region (with the lowest SPP) will not favor optimal solar power generation. Thus, this paper recommends installing the bulk of the solar facilities in the Eastern and Northern Regions which have high SPP values and SPP concentrated areas [28]. Pertinently, Figs. 4b-7b presents the conversion of the mercatorian SPP model into the corresponding spatial SPP model with the aid of the Haversine formula [46, 47, 48, 49, 50]. Precisely, these figures give the actual dimensions of SPP concentrated areas. This information is useful in mapping out the boundaries of the identified districts for the accurate installation of prospective solar power plants.

4. Conclusion

The present study has developed isodose lines in mercatorian and spatial coordinates as guides for the installation of solar facilities. The distributed SPP contour is made of multiple isodose lines showing the magnitude or variation of the SPP in the study areas, whereas the single highest isodose line formed in the distributed SPP contour characterizes the concentrated SPP. The concentrated areas are the main target for setting up high-performing solar facilities. The results show the concentrated SPP as 757.5, 635.2, 557.5, 405.9 W/m^2 for NR, ER, CR and WR, respectively. The corresponding concentrated areas are as follows: 29084.6, 15368.6, 1179.6 and 635.7 km^2, for NR, ER, CR and WR, respectively. Due to the high magnitude of the SPP and wider concen-

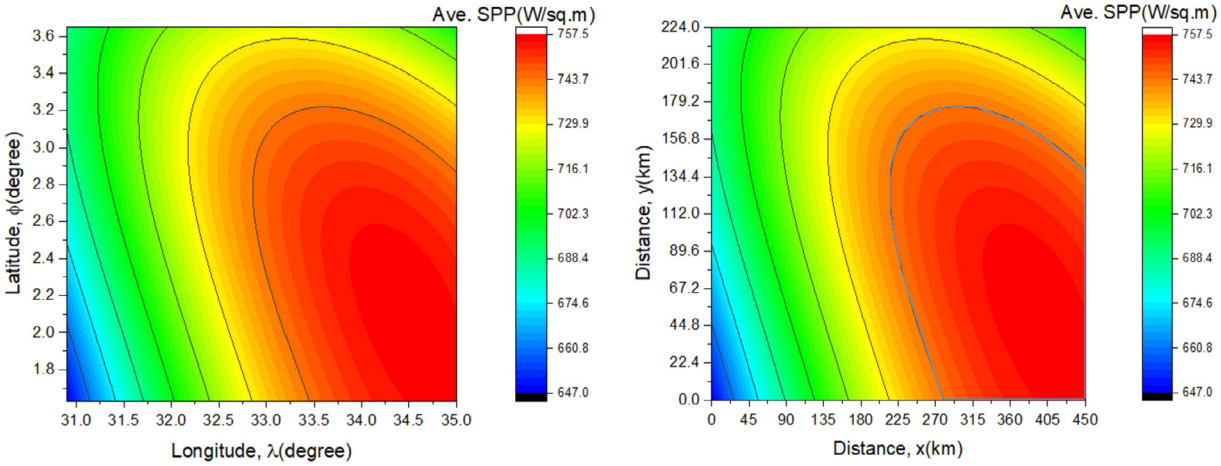

(a) Mercatorian isodoses (b) Spatial isodoses

Fig. 4. (a, b) Mercatorian and spatial distribution of solar power potential for Northern Region.

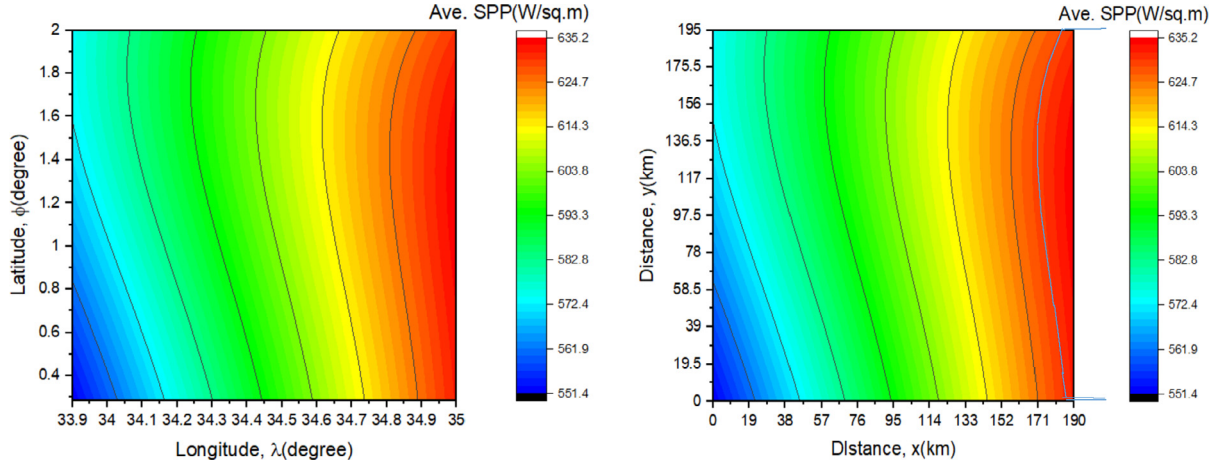

(a) Mercatorian isodoses (b) Spatial isodoses

Fig. 5. (a, b) Mercatorian and spatial distribution of solar power potential for Eastern Region.

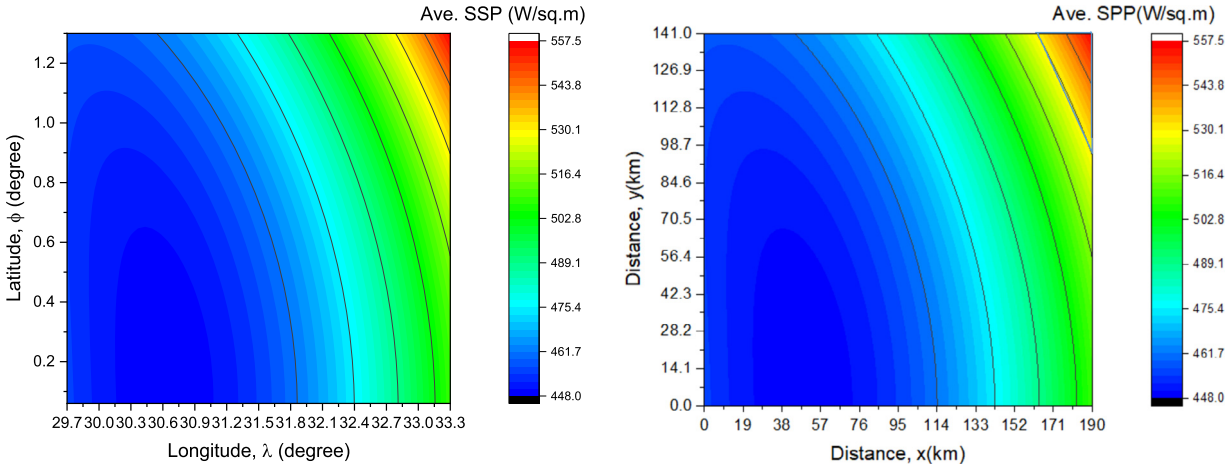

(a) Mercatorian isodoses (b) Spatial isodoses

Fig. 6. (a, b) Mercatorian and spatial distribution of solar power potential for Central Region.

Table 6. Validation of solar power potential in the study areas Figs. 12–15.

Region	Root mean square error (RMSE)			Remarks
	Previous SPP models		Present SPP model	
	Rijix and Huskley (1964)	Mubiru et al. (2007)	Present work	
NR	75.82	56.53	1.26E-06	Based on Fig. 12
ER	60.21	41.43	6.74E-06	Based on Fig. 13
CR	45.81	45.63	2.93E-05	Based on Fig. 14
WR	36.32	38.89	1.48E-05	Based on Fig. 15

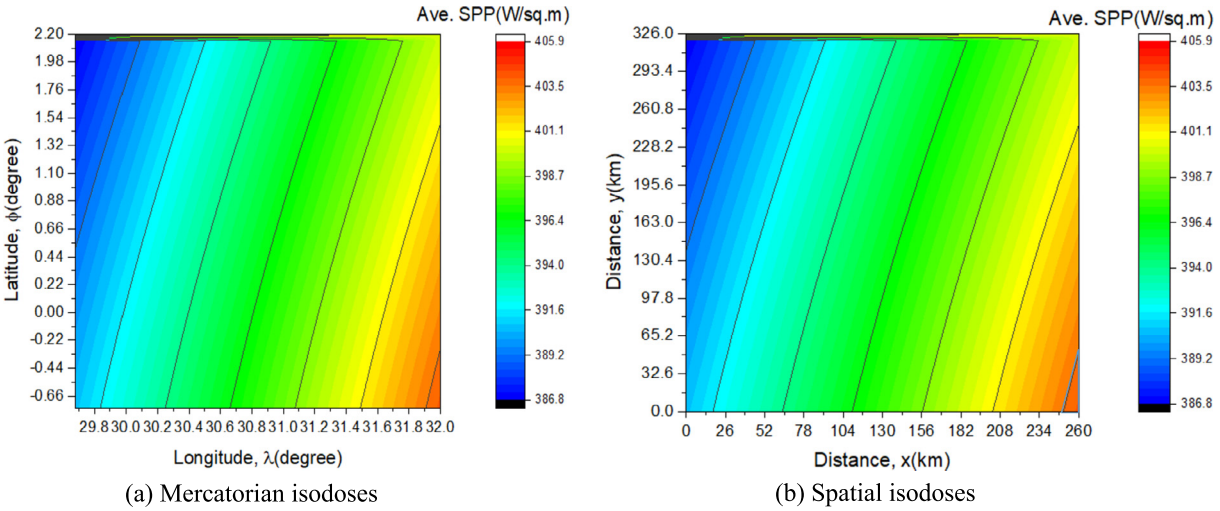

Fig. 7. (a, b) Mercatorian and spatial distribution of solar power potential for Western Region.

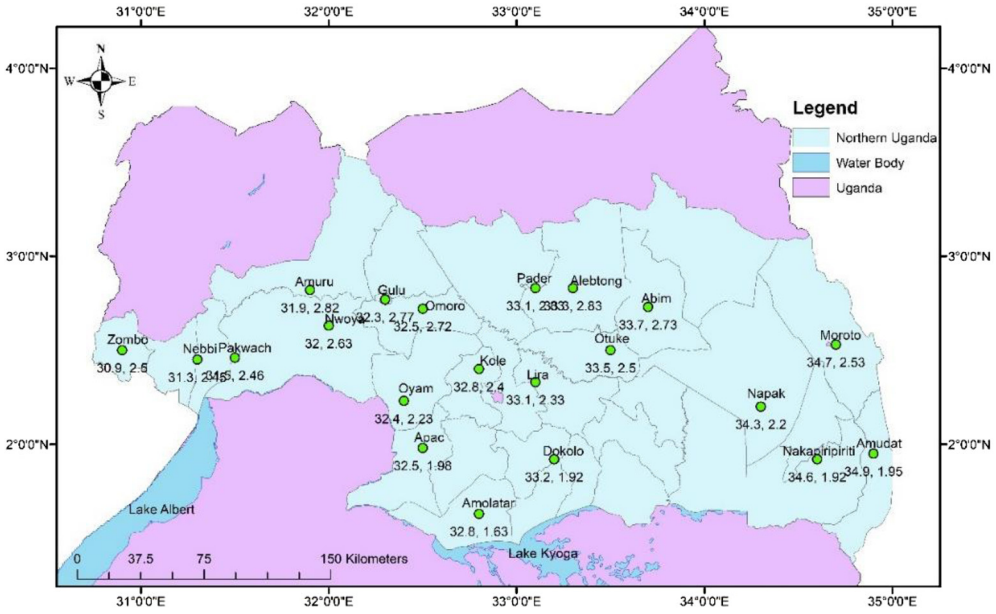

Fig. 8. SPP concentrated districts within the Norther Region.

trated areas of the SPP, it is evident that ER and NR are the most suitable home for the installation of solar facilities. Furthermore, these results show that the CR is a runner-up to ER and NR in terms of magnitude and concentrated areas of SPP. Thus, the WR region is associated with the lowest SPP and concentrated areas, thus, installation of solar facilities in WR is unprofitable. The districts found in the concentrated areas of NR are; Abim Agago, Alebtong, Amolatar, Amudat, Amuru, Apac, Dokolo, Gulu, Kaabong, Kole, Lira, Moroto, Nakapiripirit, Napak, Nebbi, Nwoya, Omoro, Otuke, Oyam, Pader, Pakwach and Zombo. Those found in the concentrated areas of ER are; Bududa, Bukwo, Kapchorwa, Kween, Manafwa, Mbale, Ngora, Serere, Soroti, Kaberamaido and Katakwi. The districts identified in the concentrated areas of the CR are Kyankwanzi, Nakaseke, Kiboga, Kayunga and Nakasongola. How-

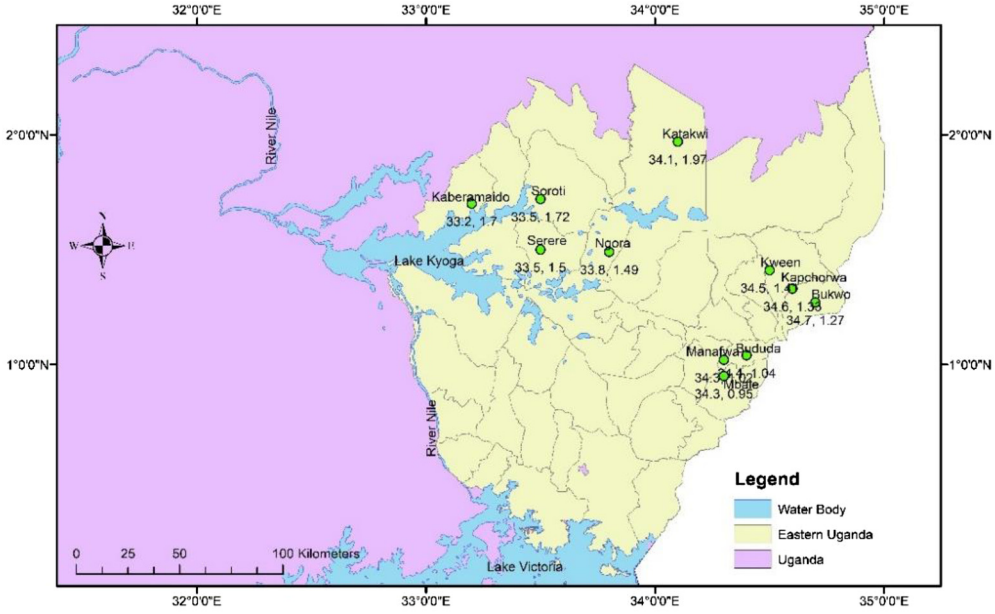

Fig. 9. SPP concentrated districts within the Eastern Region.

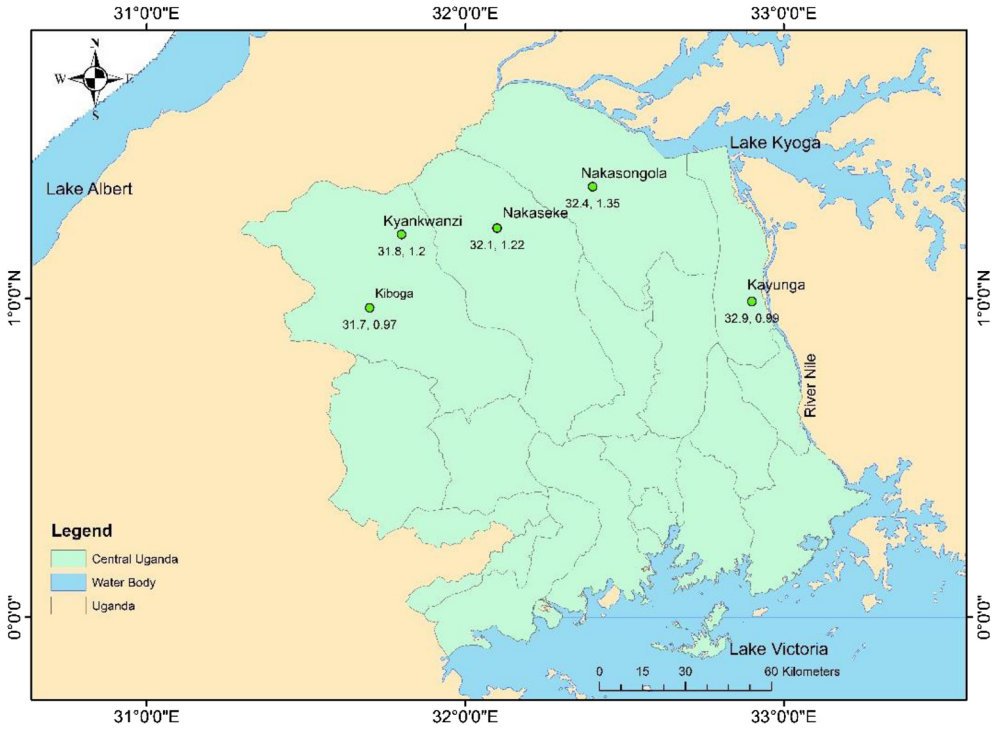

Fig. 10. SPP concentrated districts within the Central Region.

ever, the WR has Kisoro district as only the district with an appreciable SPP.

Moreover, the present SPP models in mercatorian and spatial coordinates are quite robust as they recorded negligible value of RMSE relative to previous models by Muburi et al. [10] and Rijix and Huskley [11]. Thus, the present model demonstrated a strong agreement with the measured SPP data compared to the previous models. Hence, the concentrated isodose line developed through this model is reliable for the installation of solar facilities in the study areas. The linear relationship between the SPP and clearness index in NR, CR and WR supports the fact that the atmosphere is free of pollution. However, the ER portrayed a nonlinear relationship between the SPP and clearness index indicating that the atmosphere is not free from pollution.

Furthermore, energy planners should adopt the results of this study to improve solar power generation in the study areas (NR, ER and CR). Moreover, the application of the SPP model developed in this work is limited to the present study areas; however, the extension of the methodology is possible to other study areas having similar geographic characteristics as Uganda.

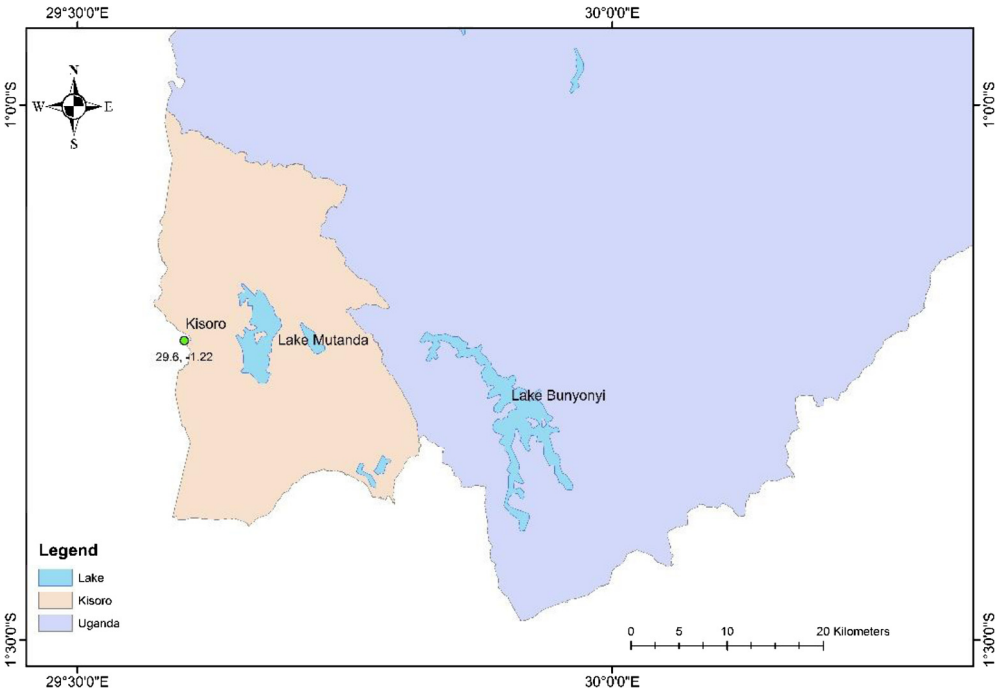

Fig. 11. SPP concentrated districts within the Western Region.

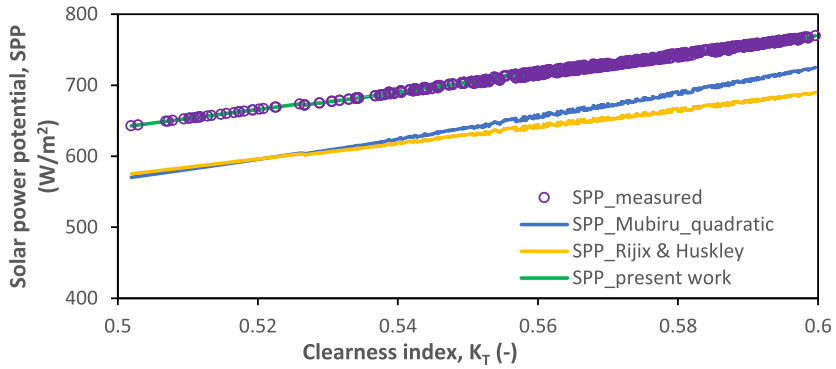

Fig. 12. Reliability of solar power potential on clearness index for Northern Region.

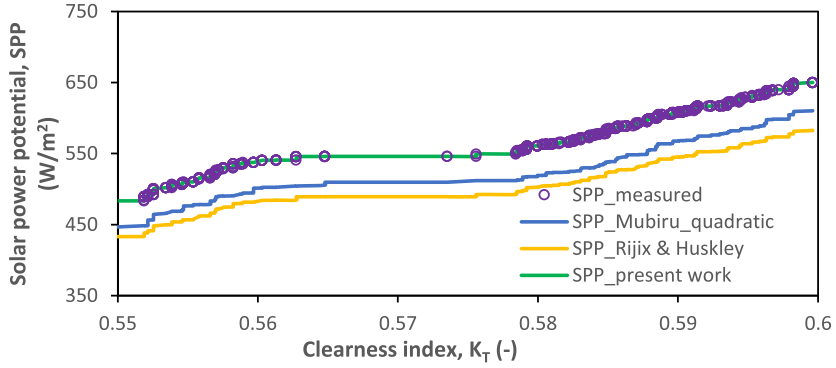

Fig. 13. Response of solar power potential to clearness index for Eastern region.

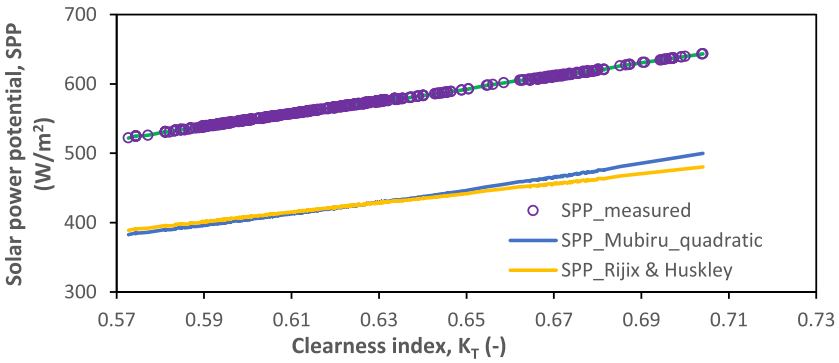

Fig. 14. Reliance of solar power potential on clearness index for Central Region.

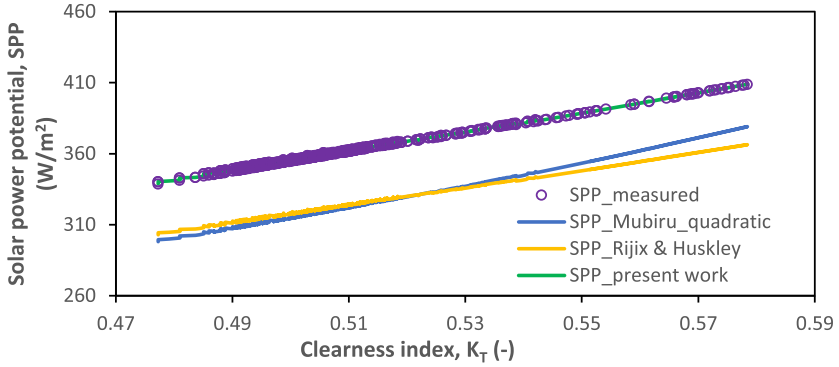

Fig. 15. Dependence of solar power potential on clearness index for Western Region.

Declarations

Author contribution statement

Stephen Ndubuisi Nnamchi: Conceived and designed the experiments; Analyzed and interpreted the data; Wrote the paper.

Mustafa Muhamed Mundu: Performed the experiments; Contributed reagents, materials, analysis tools or data.

Funding statement

This research did not receive any specific grant from funding agencies in the public, commercial, or not-for-profit sectors.

Data availability statement

Data will be made available on request.

Declaration of interests statement

The authors declare no conflict of interest.

Additional information

No additional information is available for this paper.

References

[1] N. Adeniji, J. Akinpelu, S. Adeola, J. Adeniji, Estimation of global solar radiation, sunshine hour distribution and clearness index in Enugu, Nigeria, J. Appl. Sci. Environ. Manag. 23 (2) (2019) 345–349.

[2] E. Kabir, P. Kumar, S. Kumar, A.A. Adelodun, K.H. Kim, Solar energy: potential and future prospects, Renew. Sustain. Energy Rev. 82 (2018) 894–900.

[3] T. Muneer, S. Etxebarria, E. Gago, Monthly averaged-hourly solar diffuse radiation model for the UK, Build. Serv. Eng. Res. Technol. 35 (6) (2014) 573–584.

[4] C.A. Chapman, K. Valenta, T.R. Bonnell, K.A. Brown, L.J. Chapman, Solar radiation and ENSO predict fruiting phenology patterns in a 15-year record from Kibale National Park, Uganda, Biotropica 50 (3) (2018) 384–395.

[5] O.W.K. Avellino, F. Mwarania, A.H.A. Wahab, K.T. Aime, Uganda solar energy utilization: current status and future trends, Publ. Int. J. Sci. 8 (3) (2018).

[6] S. Twaha, M.A. Ramli, P.M. Murphy, M.U. Mukhtiar, H.K. Nsamba, Renewable based distributed generation in Uganda: resource potential and status of exploitation, Renew. Sustain. Energy Rev. 57 (2016) 786–798.

[7] M. Yesilbudak, M. Çolak, R. Bayindir, A review of data mining and solar power prediction, in: 2016 IEEE International Conference on Renewable Energy Research and Applications (ICRERA), IEEE, 2016.

[8] A. Khogali, O. Albar, B. Yousif, Wind and solar energy potential in Makkah (Saudi Arabia)—comparison with Red Sea coastal sites, Renew. Energy 1 (3–4) (1991) 435–440.

[9] D. Fadare, Modelling of solar energy potential in Nigeria using an artificial neural network model, Appl. Energy 86 (9) (2009) 1410–1422.

[10] J. Mubiru, E.J.K.B. Banda, F. D'Ujanga, T. Senyonga, Assessing the performance of global solar radiation empirical formulations in Kampala, Uganda, Theor. Appl. Climatol. 87 (1–4) (2007) 179–184.

[11] D.A. Rijks, P.A. Huxley, The empirical relation between solar radiation and hours of bright sunshine near Kampala, Uganda, J. Appl. Ecol. (1964).

[12] A. Rahimikhoob, S. Behbahani, M. Banihabib, Comparative study of statistical and artificial neural network's methodologies for deriving global solar radiation from NOAA satellite images, Int. J. Climatol. 33 (2) (2013) 480–486.

[13] K. Angela, S. Taddeo, M. James, Predicting global solar radiation using an artificial neural network single-parameter model, Adv. Artif. Neural Syst. (2011).

[14] A. Sözen, E. Arcaklıoğlu, M. Özalp, N. Çağlar, Forecasting based on neural network approach of solar potential in Turkey, Renew. Energy 30 (7) (2005) 1075–1090.

[15] A.K. Yadav , S. Chandel, Solar energy potential assessment of western Himalayan Indian state of Himachal Pradesh using J48 algorithm of WEKA in ANN based prediction model, Renew. Energy 75 (2015) 675–693.

[16] T. Khatib, A. Mohamed, M. Mahmoud, K. Sopian, Modeling of daily solar energy on a horizontal surface for five main sites in Malaysia, Int. J. Green Energy 8 (8) (2011) 795–819.

[17] M. Bilgili, M. Ozgoren, Daily total global solar radiation modeling from several meteorological data, Meteorol. Atmos. Phys. 112 (3–4) (2011) 125.

[18] R. Mbiaké, A.B. Wakata, E. Mfoumou, E. Ndjeuna, L. Fotso, E. Tiekwe, J.K. Djamen, C. Bobda, The relationship between global solar radiation and sunshine durations in Cameroon, Open J. Air Pollut. 7 (2) (2018) 107–119.

[19] A.O. Onyango, V. Ongoma, Estimation of mean monthly global solar radiation using sunshine hours for Nairobi City, Kenya, J. Renew. Sustain. Energy 7 (5) (2015) 053105.

[20] D.T. Cotfas, P.A. Cotfas, E. Kaplani, C. Samoila, Monthly average daily global and diffuse solar radiation based on sunshine duration and clearness index for Brasov, Romania, J. Renew. Sustain. Energy 6 (5) (2014) 053106.
[21] T. Khatib, A. Mohamed, K. Sopian, A review of solar energy modeling techniques, Renew. Sustain. Energy Rev. 16 (5) (2012) 2864–2869.
[22] H. Li, W. Ma, Y. Lian, X. Wang, L. Zhao, Global solar radiation estimation with sunshine duration in Tibet, China, Renew. Energy 36 (11) (2011) 3141–3145.
[23] Y. Noguchi, Solar radiation and sunshine duration in East Asia, Arch. Meteorol. Geophys. Bioklimatol., Ser. B 29 (1–2) (1981) 111–128.
[24] O. Ajayi, O. Ohijeagbon, C. Nwadialo, O. Olasope, New model to estimate daily global solar radiation over Nigeria, Sustain. Energy Technol. Assess. (2014) 28–36.
[25] S.A.A. Karim, B.S.M. Singh, R. Razali, N. Yahya, Data compression technique for modeling of global solar radiation, in: 2011 IEEE International Conference on Control System, Computing and Engineering, IEEE, 2011.
[26] H.C. Bayrakç, C. Demircan, A. Keçebaş, The development of empirical models for estimating global solar radiation on horizontal surface: a case study, Renew. Sustain. Energy Rev. 81 (2018) 2771–2782.
[27] L. Wang, O. Kisi, M. Zounemat-Kermani, Z. Zhu, W. Gong, Z. Niu, H. Liu, Z. Liu, Prediction of solar radiation in China using different adaptive neuro-fuzzy methods and M5 model tree, Int. J. Climatol. 37 (3) (2017) 1141–1155.
[28] N. Mohajeri, G. Upadhyay, A. Gudmundsson, D. Assouline, J. Kämpf, J.L. Scartezzini, Effects of urban compactness on solar energy potential, Renew. Energy 93 (2016) 469–482.
[29] N. Lockart, D. Kavetski, S.W. Franks, A new stochastic model for simulating daily solar radiation from sunshine hours, Int. J. Climatol. 35 (6) (2015) 1090–1106.
[30] M. Benghanem, A. Mellit, A simplified calibrated model for estimating daily global solar radiation in Madinah, Saudi Arabia, Theor. Appl. Climatol. 115 (1–2) (2014) 197–205.
[31] P. Redweik, C. Catita, M. Brito, Solar energy potential on roofs and facades in an urban landscape, Sol. Energy 97 (2013) 332–341.
[32] K.R. Adhikari, B.K. Bhattarai, S. Gurung, Estimation of global solar radiation for four selected sites in Nepal using sunshine hours, temperature and relative humidity, J. Power Energy Eng. 1 (03) (2013) 1.
[33] V. Badescu, C.A. Gueymard, S. Cheval, C. Oprea, M. Baciu, A. Dumitrescu, F. Iacobescu, I. Milos, C. Rada, Accuracy analysis for fifty-four clear-sky solar radiation models using routine hourly global irradiance measurements in Romania, Renew. Energy 55 (2013) 85–103.
[34] T. Iizumi, M. Nishimori, M. Yokozawa, A. Kotera, N. Duy Khang, Statistical downscaling with Bayesian inference: estimating global solar radiation from reanalysis and limited observed data, Int. J. Climatol. 32 (3) (2012) 464–480.
[35] K.H. Lee, Constructing a non-linear relationship between the incoming solar radiation and bright sunshine duration, Int. J. Climatol. 30 (12) (2010) 1884–1892.
[36] R. Kumar, L. Umanand, Estimation of global radiation using clearness index model for sizing photovoltaic system, Renew. Energy 30 (15) (2005) 2221–2233.
[37] E. Couderc, Solar energy: hotspots in Tanzania, Nat. Energy 2 (7) (2017) 1.
[38] T. Ramachandra, R. Jain, G. Krishnadas, Hotspots of solar potential in India, Renew. Sustain. Energy Rev. 15 (6) (2011) 3178–3186.
[39] M. Šúri, J. Hofierka, A new GIS-based solar radiation model and its application to photovoltaic assessments, Trans. GIS 8 (2) (2004) 175–190.
[40] A. Aly, S.S. Jensen, A.B. Pedersen, Solar power potential of Tanzania: identifying CSP and PV hot spots through a GIS multicriteria decision making analysis, Renew. Energy 113 (2017) 159–175.
[41] S. Salcedo-Sanz, C. Casanova-Mateo, J. Muñoz-Marí, G. Camps-Valls, Prediction of daily global solar irradiation using temporal Gaussian processes, IEEE Geosci. Remote Sens. Lett. 11 (11) (2014) 1936–1940.
[42] Uganda: Administrative units, GeoHive, Archived from the original on 2013-05-11 (Retrieved 18 June 2013).
[43] Y. Zhang, B. Qin, W. Chen, Analysis of 40 year records of solar radiation data in Shanghai, Nanjing and Hangzhou in Eastern China, Theor. Appl. Climatol. 78 (4) (2004) 217–227.
[44] M.M. Mundu, S.N. Nnamchi, KJ. Ukagwu, Algorithmized modelling, simulation and validation of clearness index in four regions of Uganda, J. Solar Energy Res. 5 (2) (2020) 432–452.
[45] S. Nnamchi, O. Sanya, K. Zaina, V. Gabriel, Development of dynamic thermal input models for simulation of photovoltaic generators, Int. J. Ambient Energy (2018) 1–13.
[46] R.A. Azdy, F. Darnis, Use of haversine formula in finding distance between temporary shelter and waste end processing sites, J. Phys. Conf. Ser. (2020).
[47] D.A. Prasetya, P.T. Nguyen, R. Faizullin, I. Iswanto, E.F. Armay, Resolving the shortest path problem using the haversine formula, J. Crit. Rev. 7 (1) (2020) 62–64.
[48] E. Maria, E. Budiman, H. Haviluddin, M. Taruk, Measure distance locating nearest public facilities using Haversine and Euclidean Methods, IOP-J. Phys. Conf. Ser. (2020).
[49] K. Saputra, N. Nazaruddin, D.H. Yunardi, R. Andriyani, Implementation of haversine formula on location based mobile application in Syiah Kuala University, in: 2019 IEEE International Conference on Cybernetics and Computational Intelligence (CyberneticsCom), IEEE, 2019.
[50] T. Monawar, S.B. Mahmud, A. Hira, Anti-theft vehicle tracking and regaining system with automatic police notifying using Haversine formula, in: 2017 4th International Conference on Advances in Electrical Engineering (ICAEE), IEEE, 2017.
[51] F. Nestola, J.R. Smyth, Diamonds and water in the deep Earth: a new scenario, Int. Geol. Rev. 58 (3) (2016) 263–276.
[52] A.V. Matioc, Exact geophysical waves in stratified fluids, Appl. Anal. 92 (11) (2013) 2254–2261.
[53] A.P. Trishchenko, L. Garand, Observing polar regions from space: advantages of a satellite system on a highly elliptical orbit versus a constellation of low Earth polar orbiters, Can. J. Remote Sens. 38 (1) (2012) 12–24.
[54] NASA Prediction of world energy resources, power data access viewer, https://power.larc.nasa.gov/data-access-viewer/, 2018. (Accessed 13 June 2021).
[55] Department of Physics, Makerere University, Meteorological On-Station Data on Insolation, 2018.